



### Key Points:

- Earthquake relocations constrain the locations and kinematics of previously unrecognized faults, including the Connector fault, in SW Yukon
- Slip partitioning of thrust and strike-slip motion is observed on these predominantly shallow faults
- Active tectonics in SE Alaska and SW Yukon are characterized by a corridor of transpressional deformation bounded by regional-scale faults

### Supporting Information:

Supporting Information may be found in the online version of this article.

### Correspondence to:

K. M. Biegel,  
katherine.biegel@ucalgary.ca

### Citation:

Biegel, K. M., Gosselin, J. M., Dettmer, J., Colpron, M., Enkelmann, E., & Caine, J. S. (2024). Earthquake relocations delineate a discrete fault network and deformation corridor throughout southeast Alaska and southwest Yukon. *Tectonics*, 43, e2023TC008140. <https://doi.org/10.1029/2023TC008140>

Received 11 OCT 2023

Accepted 29 APR 2024

### Author Contributions:

**Conceptualization:** K. M. Biegel, J. M. Gosselin, J. Dettmer  
**Data curation:** K. M. Biegel  
**Formal analysis:** K. M. Biegel  
**Investigation:** K. M. Biegel, J. M. Gosselin  
**Methodology:** K. M. Biegel, J. M. Gosselin, J. Dettmer  
**Project administration:** J. Dettmer  
**Software:** K. M. Biegel  
**Supervision:** J. Dettmer  
**Visualization:** K. M. Biegel  
**Writing – original draft:** K. M. Biegel, J. M. Gosselin

© 2024 The Authors.

This is an open access article under the terms of the Creative Commons Attribution-NonCommercial License, which permits use, distribution and reproduction in any medium, provided the original work is properly cited and is not used for commercial purposes.

## Earthquake Relocations Delineate a Discrete Fault Network and Deformation Corridor Throughout Southeast Alaska and Southwest Yukon

K. M. Biegel<sup>1</sup> , J. M. Gosselin<sup>2</sup> , J. Dettmer<sup>1</sup> , M. Colpron<sup>3</sup> , E. Enkelmann<sup>1</sup> , and J. S. Caine<sup>4</sup> 

<sup>1</sup>Department of Earth, Energy, and Environment, University of Calgary, Calgary, AB, Canada, <sup>2</sup>Geological Survey of Canada - Pacific, Natural Resources Canada, Sidney, BC, Canada, <sup>3</sup>Yukon Geological Survey, Whitehorse, YT, Canada,

<sup>4</sup>U.S. Geological Survey, Geology, Denver, CO, USA

**Abstract** Deformation in southeastern Alaska and southwest Yukon is governed by the subduction and translation of the Pacific-Yakutat plates relative to the North American plate in the St. Elias region. Despite notable historical seismicity and major regional faults, studies of the region between the Fairweather and Denali faults are complicated by glacial coverage and the remote setting. In the last decade, significant improvements have been made to the density of regional broadband seismometer networks. We relocate more than 5,000 earthquakes between 2010 and 2021 in the region of southeastern Alaska and southwestern Yukon utilizing these improved seismic networks. With reductions in catalog uncertainty, particularly in depth, we quantify the thickness of the seismogenic layer in the crust throughout the region and locate seismicity on a shallow network of upper-crustal faults. Relocated earthquakes, combined with an updated focal-mechanism catalog, permit estimating and classifying motion of active faults. This includes mapping the Totschunda-Fairweather “Connector” fault, which plays an important role in explaining regional deformation, and identifying new faults like the Kathleen Lake fault. We draw similarities between our seismic observations and simplified conceptual models of regional tectonics, which describe a dominant transpressional regime and localized slip partitioning. Our results support a hypothesis where current deformation is taking place on a well-defined and evolved network of shallow faults in the corridor between the Totschunda-Fairweather “Connector” and Denali faults.

**Plain Language Summary** Southeastern Alaska and southwest Yukon are actively deforming due to their position at the collision of multiple tectonic plates as the Pacific plate and the Yakutat microplate collide with the North American plate. The region has a large number of significant earthquakes and many mapped faults. Traditional methods of identifying faults, such as field mapping or remote satellite imagery, are complicated due to the remote setting, large glaciers, and mountainous terrain. Here, we analyzed more than 5,000 earthquakes from 2010 to 2021 to better understand how deformation occurs and where active faults are located. Our results show that earthquakes occur on a shallow network of faults, confirming models of an actively deforming and uplifting continental crust. We can map and classify motion on new faults, such as the “Connector” fault, showing that deformation transfers inland hundreds of kilometers from the colliding tectonic plates to the Denali fault in central Alaska. Our results support evidence of an evolving fault system, with deformation occurring on a well-defined network of shallow faults in the corridor between the plate boundary and the Denali fault.

### 1. Introduction

We aim to understand how stress is transferred into continents at highly oblique subduction-related collision zones. Our focus is on deformation caused by the ongoing subduction of the Pacific-Yakutat plates underneath the North American plate in southern Alaska (Plafker, 1987) that results in an oblique collision of the Yakutat plate corner into southeast Alaska and southwest Yukon (Figure 1). The Yakutat-North American plate interactions drive regional deformation and have formed the St. Elias Mountains. The St. Elias is heavily glaciated, characterized by significant seismicity (Bruhn et al., 2012; Doser, 2012, 2014; Meighan et al., 2013) and extremely high rates of rock uplift, erosion, and exhumation that have been compared with the eastern and western Himalayan syntaxes (Enkelmann et al., 2009; Koons et al., 2022). Unlike the Himalayan syntaxes, which appear to be steady in their location of focused deformation and erosion, the St. Elias Mountains are more dynamic due to an effective interplay of changing tectonics and surface processes (Enkelmann et al., 2015). While most of the

**Writing – review & editing:**

K. M. Biegel, J. M. Gosselin, J. Dettmer,  
M. Colpron, E. Enkelmann, J. S. Caine

crustal-scale deformation occurs southwest of the plate boundary, within the deforming Yakutat basement and its sedimentary cover, there is significant seismicity occurring inboard of the plate boundary (Figure 2). However, the spatial pattern and relationship to known and unknown faults are unclear due to the remote location, heavy glaciation, and international boundary in the region.

An important regional tectonic question regards the existence and nature of the “Connector” fault (Kalbas et al., 2008; Richter & Matson, 1971). This hypothesized fault may connect the dextral Fairweather transform plate boundary on the eastern edge of the Yakutat microplate with the dextral Totschunda fault, effectively coupling seismicity and stress accumulation on the plate margin to the central section of the Denali fault in Central Alaska. The Connector fault was proposed on the basis of similar fault alignment between the Totschunda and Fairweather faults (Richter & Matson, 1971), geodynamic models (Koons et al., 2010), and accommodation of differences in slip rates between the connected faults (Elliott & Freymueller, 2020). The snow and ice cover prevent direct field observations and present a challenge to some airborne and satellite remote-sensing geophysical analyses, such as Curie-depth estimation where gaps in global Curie-depths models can be seen in the St. Elias region (Li et al., 2017). The wedge-shaped nature of the colliding Yakutat plate (Christeson et al., 2010; Van Avendonk et al., 2013) suggests an increase in plate coupling over time. Increased coupling suggests that stress that is transferred inboard of the plate boundary also increases, resulting in strain inboard. Revealing how strain is distributed and manifested in discrete faults is a primary goal of this study.

During the last decade, there has been a large increase in the number of high quality broadband seismic stations in the study area. We use these improved data for earthquake relocation and interpret the result in combination with a synthesis of available earthquake focal mechanism inversions. With these data and results, we are able to reveal active faults and define fault motion to understand the regional-scale pattern of seismicity. Furthermore, our analysis places constraints on the seismogenic thickness of the crust due to improvements in earthquake depth estimates.

## 2. Tectonic Setting

The Northern Canadian Cordillera formed by accretion of complex terranes resulting in large-scale strike-slip faults, such as the Tintina and Denali faults, which accumulated hundreds of kilometers of displacement (Lowey, 1998; Waldien et al., 2021). On the present continental margin, the dextral Fairweather fault serves as the plate boundary between the Yakutat and North American plates with a current GPS-derived block model estimated rate of motion of approximately 35.5 mm/yr (Figure 1; Elliott & Freymueller, 2020). The Fairweather transform boundary transitions into the Chugach–St. Elias fault along the northern boundary of the Yakutat microplate, which merges with the Aleutian megathrust systems to the southwest (Figure 1a).

The Yakutat microplate (Figure 1a) is connected with the Pacific plate (Transition fault) and moves at a rate of approximately 53 mm/yr toward the northwest, although there is an azimuthal difference of 15° between their motions (Elliott & Freymueller, 2020; Plafker, 1987). Composed primarily of oceanic basalt, which is significantly thicker (15–30 km) and more buoyant in comparison to the Pacific plate (Plafker, 1987), the Yakutat microplate originated approximately at 55 Ma from oceanic crust approximately 600 km to the southeast of its current position, along the western margin of British Columbia (Bruns, 1983). As the Yakutat microplate has progressed along the Queen Charlotte–Fairweather transform system to its modern-day position at the corner of Alaska and Yukon, it has accumulated a series of both depositional sedimentary layers and accretionary blocks from the North American margin (Plafker, 1987). The thick Yakutat microplate causes flat-slab subduction under southern Alaska with slab remnants and deformation that can be detected in seismic imaging studies as far north as the Central Denali fault in central Alaska (Figure 1a; Eberhart-Phillips et al., 2006).

Several large-magnitude complex earthquakes have occurred along the portion of the Fairweather fault that bounds the Yakutat microplate (Figure 1a). In September 1899, a series of large-magnitude earthquakes occurred in Yakutat Bay. This series included a magnitude (M) 8.1 thrust event on September 6th in the Pamplona fault zone and a M 8.2 event on September 10th, which generated over 14 m of surface uplift in the region of Yakutat Bay and triggered a tsunami wave approximately 12 m tall (Plafker & Thatcher, 2008; Tarr & Lawrence, 1912). It was suggested that this larger event was a multi-fault slip event, triggered on local reverse faults, in a region with high strain-partitioning (Walton et al., 2022). In 1958, there was an M 7.9 event that triggered the destructive tsunami in Lituya Bay and ruptured between 250 and 370 km of the Fairweather fault (Davis & Sanders, 1960;

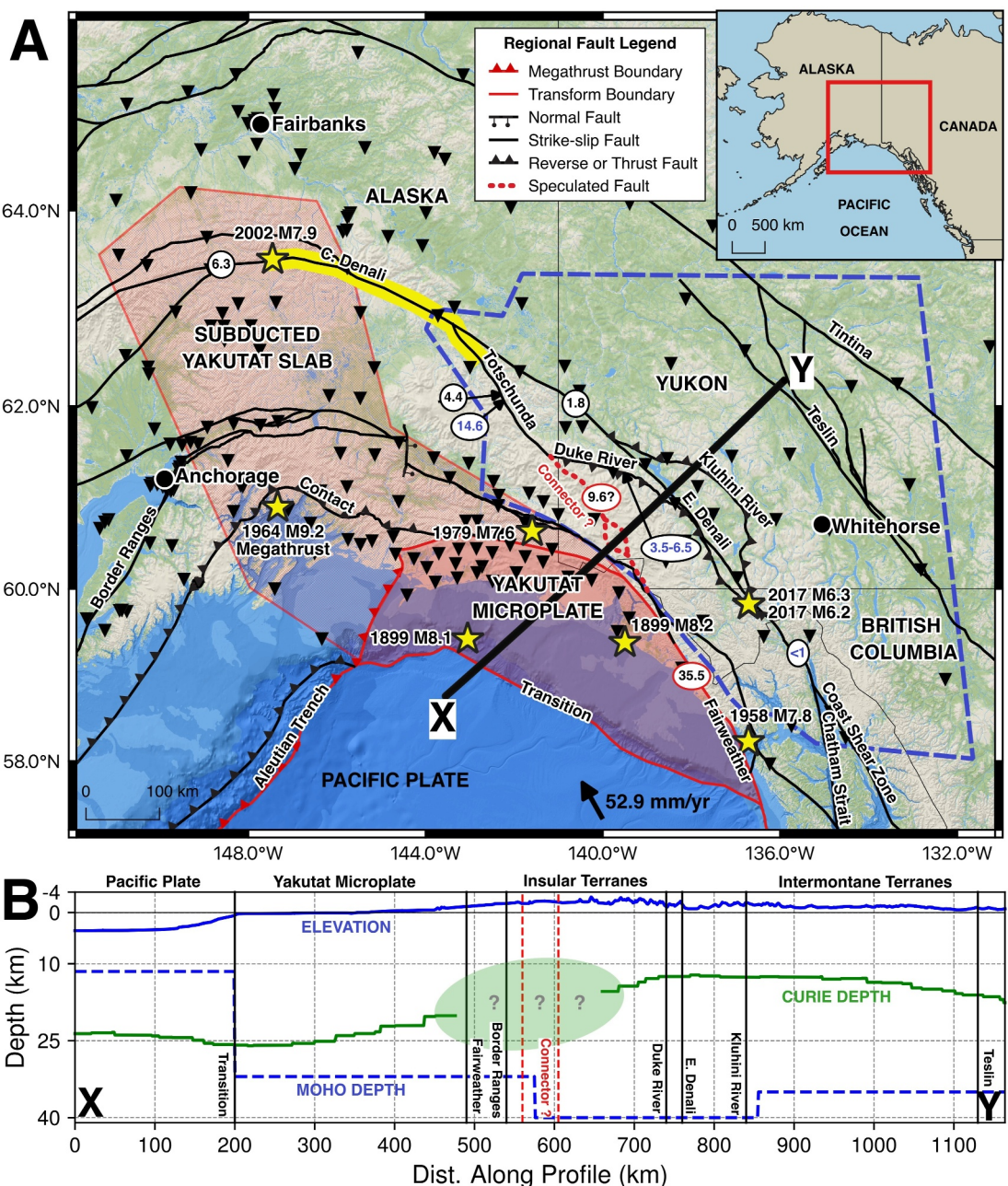


**Figure 1.** Regional tectonic setting of southeast Alaska and southwest Yukon. (a) Geometry of the Yakutat plate (red polygon) with subducted slab (light red polygon; Eberhart-Phillips et al., 2006) including major regional faults (black; Colpron & Nelson, 2020), the Connector fault (red dashed line), Pacific plate motion relative to North America (arrow; Elliott & Freymueller, 2020), annual fault slip-rates (mm/yr) taken from GPS-derived block models (ovals with black text; Elliott & Freymueller, 2020) and aerial-imagery derived geomorphological estimates (ovals with blue text; Marechal et al., 2018), notable historical earthquakes (yellow stars; U. S. Geological Survey, 2022) with 2002 Denali Earthquake rupture extent (yellow), seismic stations (triangles), and the area of seismicity considered in this study (blue dashed line). (b) Cross-section SW-NE (XY) across the Yakutat and portions of the North American Cordillera showing elevation (blue), Moho depth (blue dashed; Audet et al., 2020; Estève et al., 2021), and Curie depths (green; Li et al., 2017). The green oval indicates a gap in the global Curie-depth models. Tectonic units are labeled along with major regional-scale faults indicated by vertical lines.

Doser, 2010; Stauder, 1960). Finally in 1979, there was a series of strike-slip and low-angle thrust events in the Pamplona fault zone (Doser et al., 1997; Doser & Lomas, 2000).

Inboard of the Yakutat-North American plate boundary, the dextral Denali fault system stretches from central Alaska to British Columbia. Over its history, there have been 370–480 km of accumulated slip (e.g., Lowey, 1998;

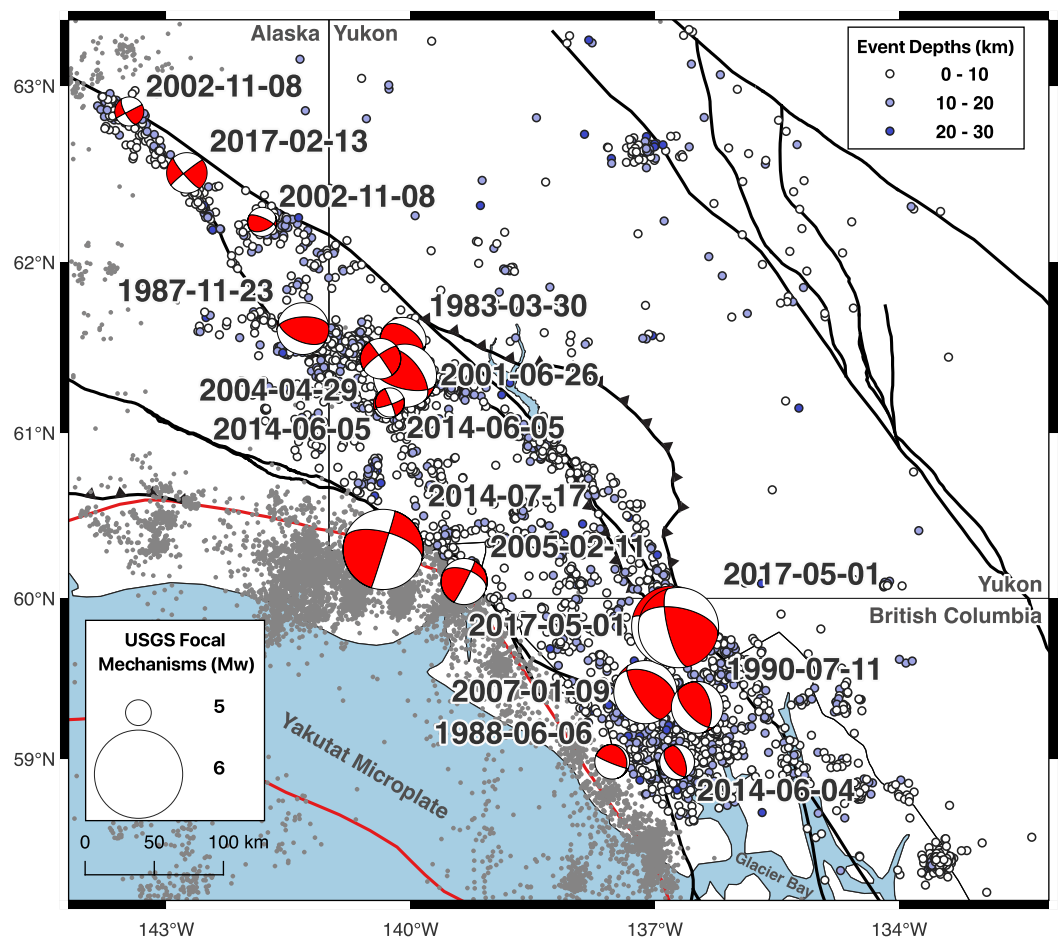


**Figure 2.** Comprehensive catalog (ComCat) seismicity (U.S. Geological Survey, 2022) for the region of study (blue dots) showing all events magnitude ( $M$ ) greater than 1.5 occurring from 2010 through 2021 color-coded by depth. Large magnitude ( $M > 5$ ) earthquakes are shown with focal mechanisms size-scaled by moment magnitude ( $M_w$ ) and labeled by associated event dates. Notable regional-scale faults are shown in black. Regional seismicity in the ComCat excluded from our study is shown in gray (for  $M > 1.5$ ).

Waldien et al., 2021). The Denali fault is divided into Western, Central, and Eastern segments (Figure 1a). The Central Denali, in central Alaska, is the most seismically active segment with a GPS-derived slip rate of 6.3 mm/yr (Figure 1a; Elliott & Freymueller, 2020). In 2002, the  $M 7.9$  Denali earthquake ruptured over 340 km of the Central Denali fault before splaying southward onto the Totschunda fault, effectively side-stepping the Eastern Denali fault in southwest Yukon (Eberhart-Phillips et al., 2003; Haeussler et al., 2004). The Eastern Denali fault, which extends through southwest Yukon, exhibits lower slip rates. GPS analysis places motion on the Eastern Denali fault at 1.8 mm/yr (Elliott & Freymueller, 2020), although geomorphological constraints show that motion on the Eastern Denali fault decreases southward and is less than 1 mm/yr (Marechal et al., 2018) where it splits into the Coast shear zone and the Chatham Strait fault (Figure 1a). Given low estimated slip rates and limited recorded seismicity, studies have suggested that the Eastern Denali fault is a regional stress boundary while active deformation occurs on other faults (Choi et al., 2021).

The region between the Fairweather and Denali faults is characterized by high topography and pervasive snow and ice-sheet coverage that impedes geological mapping and remote-sensing analyses. Known faults in this region include the Totschunda and Duke River faults. The Totschunda fault is a dextral strike-slip fault which notably ruptured in the 2002 Denali earthquake (Figure 1a; Eberhart-Phillips et al., 2006). There are varied estimates of motion on the fault, ranging from 4.4 to 14.6 mm/yr (Elliott & Freymueller, 2020; Marechal et al., 2018), although generally the Totschunda fault is actively linked to the Central Denali fault. Due to the alignment of the Totschunda fault with respect to the plate margin further south, a speculated Totschunda-

Fairweather connection (named the Connector fault) is believed to accommodate strain in the region (Kalbas et al., 2008; Richter & Matson, 1971). Orogenic-scale block models constrained by geodetic data require the Connector fault to accommodate 9.6 mm/yr of slip in order to explain differences in slip rates between the Denali and Fairweather faults (Figure 1; Elliott & Freymueller, 2020). Alternatively, diffuse distributed deformation rather than a discrete fault surface has been suggested (Marechal et al., 2015).

The Duke River fault is a high-angle reverse fault that forms the boundary between the Alexander and Wrangellia terranes (Cobbett et al., 2016) and today connects the Totschunda fault to the southern segment of the Eastern Denali fault (Figure 1a; Dodds & Campbell, 1992). Studies of the Duke River fault show that it is predominately a thrust fault that has accommodated deformation as far back as the Cretaceous and still accommodates brittle-regime deformation (Cobbett et al., 2016). In some areas of the fault, the motion has a slight dextral obliquity (Cobbett et al., 2016). Geomorphological estimates place shortening at 3.5–6.5 mm/yr (Marechal et al., 2018). The 2017 St. Elias earthquake sequence occurred at the southern terminus of the Duke River fault, likely in a strain-partitioned area between the Duke River and Denali faults (Figure 1a; He et al., 2018; Choi et al., 2021).

### 3. Methods and Data

Event-pair double-difference relocation (Waldhauser & Ellsworth, 2000) is a relative earthquake hypocenter location method used to produce relocation catalogs from differential travel times. The method exploits similar ray paths between proximal event pairs to better resolve faults. It predominantly improves relative locations, but can also improve absolute locations (Menke & Schaff, 2004). Double-difference relocation can utilize phase-arrival picks from catalogs and differential travel times from waveform cross-correlation methods (Shearer, 1997). The computation of cross-correlation differential arrival times can be further improved by Shannon-Nyquist up-sampling (Shearer, 1997), which is applied here. The computation of precise cross-correlation-based times is important to achieve relocation with low uncertainty. Prior data weights are defined by phase-arrival catalog weights and by cross-correlation coefficients, depending on the data type. The method relies on regularization (specifically, damping) in order to numerically stabilize the inversion procedure. Location errors are estimated using a statistical resampling approach (Shearer, 1997; Waldhauser & Ellsworth, 2000). Using random samples drawn with replacement from the observed residual distribution of the relocation catalog, we resample the differential-time data and relocate the catalog. We perform 250 bootstrap iterations, with the cumulative results allowing for estimating the relocation catalog uncertainty.

We relocate the Advanced National Seismic System (ANSS) comprehensive catalog (ComCat) of earthquake events (Figure 2; U.S. Geological Survey, 2022) for 6,010 events from January 2010 through December 2021 using observations from 359 seismic stations in Alaska and Canada. Figure 3 shows the relocated earthquake catalog. As our study is focused on crustal deformation, only seismicity with a cut-off depth of 30 km depth is considered, eliminating potential subduction-related events from the Yakutat microplate and limiting our study to the overriding crustal seismicity. Furthermore, seismicity with a magnitude threshold greater than 1.5, which is higher than the magnitude of completeness of the catalog which, in the study area, is less than M 1 (Meighan et al., 2013), is selected due to the need for at least eight arrival observations for each event. The earthquakes are relocated with a Python software implementation of the event-pair double-difference relocation algorithm. The ComCat has 140,186 phase arrivals, including 100,265 P arrivals and 39,321 S arrivals. Multiple velocity models (Fogleman et al., 1993; Herrmann et al., 2011; Ma & Audet, 2017; Schaeffer & Lebedev, 2014) were tested for minimal travel time residuals and raytracing feasibility. Due to the pseudo ray bending used in the relocation software, velocity models with a sharp Moho led to significant gaps in possible event-station separations, limiting the data that could be used in the relocation problem. Because of this raytracing limitation, we use a nine-layer 1D gradated velocity model (Fogleman et al., 1993) used in the creation of the regional catalog. Beyond having the largest range in possible event-station separation, relocations with this velocity model show improved travel time residuals (1.568–1.501 s), indicating improvements in absolute location when compared to the starting ComCat locations. As we have discussed in our description of the tectonic setting, this region is complex and variable. A 1D velocity model cannot capture this complexity in full, and as such, the final relocations will be dependent on these velocity uncertainties.

Event-pair selection requires a minimum of eight common stations and a maximum of 15 km inter-event separation. There are 31,898 selected event pairs with an average inter-event distance of 4.5 km. We use differential time picks for both P and S arrivals from the ComCat arrival catalog for relocation. After pairing, there are

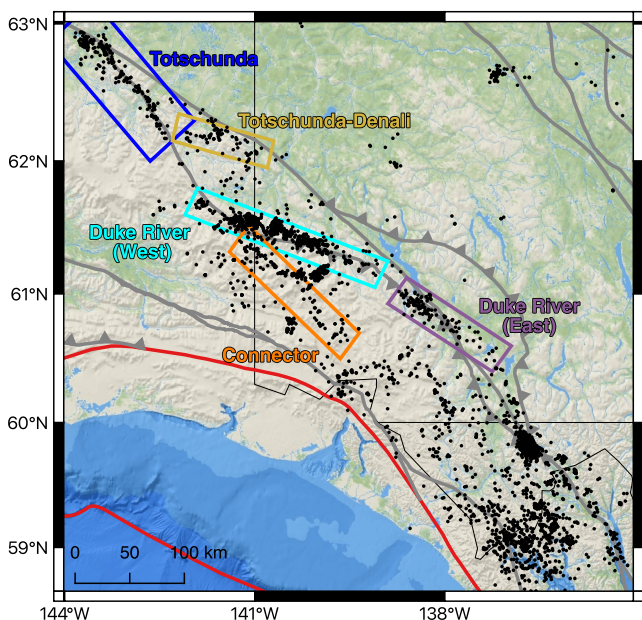


**Figure 3.** Earthquake relocations (black dots) plotted over regional faults (gray and red lines). Boxes color-coded to existing or proposed fault names indicate regions of the relocated catalog used for bootstrap uncertainty estimate (Table 1) and seismogenic thickness calculations (Table 2).

335,132 catalog P differential times and 125,117 S differential times. We compute waveform cross-correlations on 10 $\times$  upsampled waveforms downloaded through Incorporated Research Institutions for Seismology (IRIS). For quality control, we impose a threshold cross-correlation coefficient of 0.8 to retain cross-correlation differential times in the final data set. From cross-correlations, we gain 235,724 P differential times and 377,504 S differential times. Catalog data are weighted at 1.0, while cross-correlation data are weighted by correlation coefficient (between 0.8 and 1.0). After event-pairing, there are 1,073,477 differential time data points.

For double-difference relocation, we perform no clustering of events, locating all seismicity as a single cluster and starting from the network-defined event locations. We further limit the centroid-station separation to 500 km limiting data to 1,063,674 data points (99.1% of paired data) with 5,691 events retained. Relocation uses an iterative least-squares inversion (Paige & Saunders, 1982). To relocate, we perform two sets of five inversion iterations with relocation parameters consistent within sets. For the first set, cross-correlation data is down-weighted to 0.05, while catalog data is weighted at 0.9. We apply a dynamic cutoff for catalog data above 5 standard deviations. For the second relocation set, these parameters are reversed with 0.9 weights for cross-correlations with the same dynamic cutoff and 0.05 weights for catalog data. In choosing these relocation parameters, we aimed to retain both the largest number of events and the largest amount of data. The damping parameters were consistent across sets and determined using an automated L-curve criterion test to select a damping weight consistent with the statistics of data noise (Aster et al., 2018).

In addition to earthquake relocation, we present a synthesis of earthquake focal mechanisms from various sources, including the International Seismological Center (ISC, Lentas et al., 2019), the ANSS-ComCat, Saint Louis University (Herrmann et al., 2011), and a recent catalog of 374 additional focal mechanisms for small-magnitude regional events (Gosselin et al., 2023). The earthquake focal mechanisms in this compiled catalog vary in quality based on a range of factors including the data type used to estimate the mechanisms (e.g., first-motion vs. waveforms), seismic velocity models, and inversion methodologies. As the compiled focal mechanisms are used qualitatively to guide our interpretation of relocated regional seismicity, and uncertainties in focal mechanism solutions are generally not available for many events, we adopt a simple and pragmatic approach to interpret this catalog based primarily on event magnitude (as illustrated in Figure 4). It is reasonable to assume higher-quality solutions for larger-magnitude events. Inversions for such events typically consider seismic waveform data and/or polarity data of higher signal-to-noise ratio (for more accurate polarity determination) as well as measurements from additional (more distant) stations that provide superior angular sampling of the focal sphere (e.g., Hardebeck & Shearer, 2002; Vasyura-Bathke et al., 2020). This approach provides uniformity in our interpretation of the catalog, which has been compiled from variable sources. Small-magnitude events only reinforce and guide our interpretation where data are sparse.

#### 4. Results

After relocation, 5,536 events (92% of the initial catalog) are retained (Figure 3). Overall improvement in relative earthquake locations is demonstrated by a reduction in event-pair residuals from 667 to 431 ms for catalog differential times (a 31.8% reduction) and 820 to 108 ms for cross-correlation differential times (an 86.8% reduction). Furthermore, we observe an improvement in absolute uncertainty by reducing the root mean square (RMS) travel time residuals from 1.568 to 1.501 s, which indicates the catalog overall has lower absolute uncertainty when relocated with the same velocity model used to generate locations. The number of data points retained in the final relocation is 901,306 data which is 84.5% of the starting relocation differential times.

There are no uncertainty estimates for the location parameters for many events in the original ComCat event origins. As discussed in the previous section, we employ 250 iterations of bootstrap sampling to estimate relative earthquake location uncertainties for clusters along certain faults. We present the mode of the 95% confidence

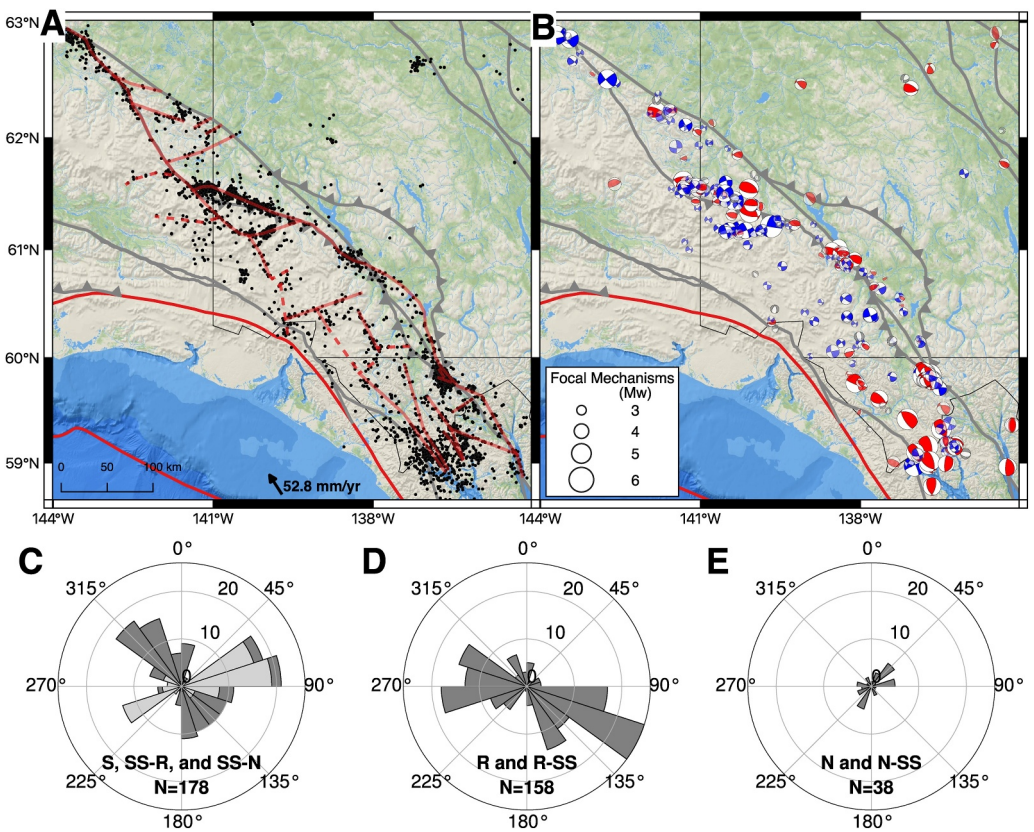


**Figure 4.** (a) Earthquake relocations (black dots) with interpreted active faults (red transparent lines). Uncertainty is shown using dashed lines. Gray and bright red lines indicate major regional faults and plate boundaries. Yakutat motion indicated by arrow (Elliott & Freymueller, 2020). Thin black lines show international and territorial boundaries. (b) Focal mechanism catalog showing strike-slip (blue), reverse (red), and normal (gray) events. Focal mechanisms are size-scaled by moment magnitude, and focal mechanisms with  $M < 4$  and  $M < 3$  are progressively more transparent. Fault strike orientations from focal mechanisms for (c) strike-slip, including strike-slip (SS), strike-slip reverse (SS-R), and strike-slip normal (SS-N); (d) reverse, including reverse (R) and reverse strike-slip (R-SS); and (e) normal, including normal (N) and normal strike-slip (N-SS) earthquakes (Alvarez-Gomez, 2019). Strike-slip earthquakes are further categorized into dextral events (dark gray) and sinistral events (light gray).

intervals for the bootstrap samples (Table 1) for various geographic locations (Figure 3). We observe consistent uncertainties in all three spatial directions between 0.5 and 2.1 km. Uncertainties in longitude (X) are generally the largest, likely due to rounding errors from high latitude unit conversions. Uncertainties in latitude (Y) range from 0.62 km in the Connector fault region to 1.00 km along the Totschunda fault. Overall, depth uncertainties (Z) are generally the smallest, partly because of the large number of S-wave cross-correlational data used in the relocation. In addition, we note a directional bias in data quality due to station coverage and existing catalog phase picks. Figures showing individual event confidence intervals in the seismicity zones outlined in Figure 3 and Table 1 can be found in the supplement.

**Table 1**

95% Confidence Intervals (CI) for Relative Location Uncertainties Based on Bootstrapping for Zones of Seismicity in the Relocated Catalog

Zone of seismicity	95% CI location uncertainty (km)		
	X	Y	Z
Totschunda	1.05	1.00	0.67
Totschunda - Denali Corridor	1.07	0.83	0.52
Duke River (West)	0.91	0.82	0.82
Connector	0.57	0.62	0.61
Duke River (East)	2.09	0.71	0.57

Because of improved seismic instrumentation in the region, we can perform seismogenic depth analysis on the relocated events and remove artifacts from the starting catalog (Figure 5). Due to challenges in resolving earthquake depths, the ComCat has significant artifacts in the distribution of event depths at 0, 1, 5, and 10 km due to manual fixed depth assignments by seismic analysts. A comparison of relocated depths with the existing catalog can be seen in Figure 5, plotted over an east-west profile of the entire catalog and a depth histogram. Similar to previous studies, we assume that the depth comprising 90% of the distribution of seismicity is representative of the seismogenic layer

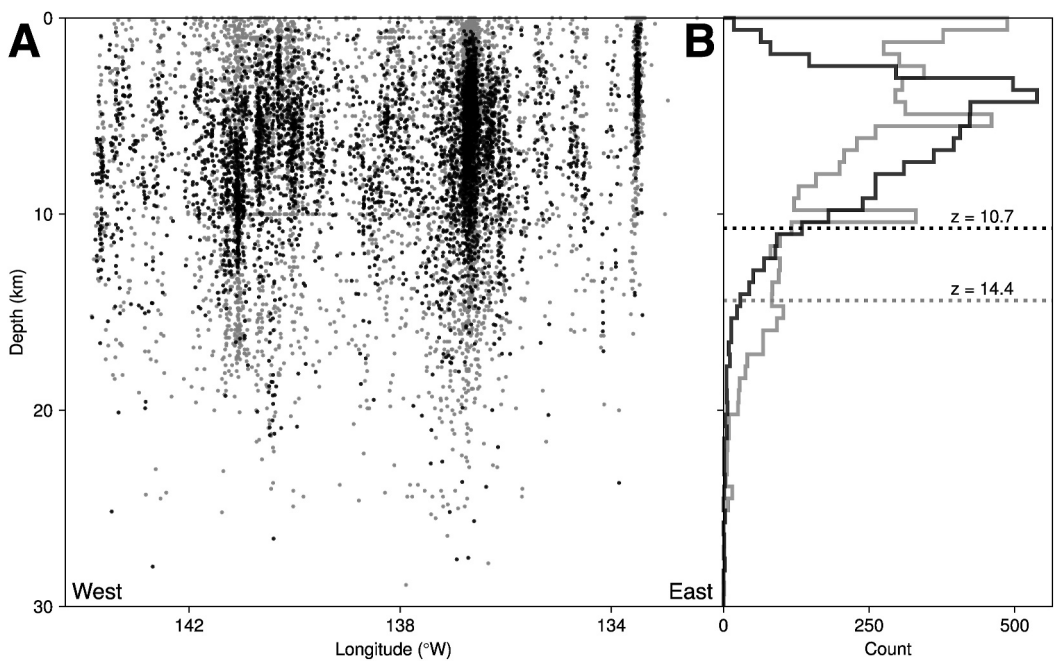


**Figure 5.** (Left) Depth profile west to east of Comprehensive catalog events (gray dots) plotted alongside relocated earthquake catalog (black dots). (Right) Histograms of event depths for the starting catalog (gray) and relocated events (black) with effective seismogenic layer thickness (depth comprising 90% of seismicity) indicated by the respective dotted lines. The seismogenic layer thickness in the study region is 10.7 and 14.4 km based on the relocated and original catalogs, respectively. For the original catalog, we see location artifacts for unknown depths at 1, 5, and 10 km depths.

thickness of the upper crust (Furlong & Atkinson, 1993; Miller & Furlong, 1988; Smith-Konter et al., 2011). We observe that this layer is significantly thinner for the relocated catalog (10.7 km) compared to the original catalog (14.4 km). Relocated depths show a convergence of seismicity to shallow depths, with the median depth of seismicity being 5.9 km.

## 5. Discussion

The map view of the relocated earthquake catalog highlights several linear features that permit the interpretation of fault locations at depth and their significance within a regional tectonic context. Furthermore, using the extended focal mechanism catalog, we are able to characterize the motion on these faults. We begin by discussing regional patterns in the orientations of structures, then show how local-scale faults fit into a regional tectonic interpretation, and finally discuss estimates of seismogenic layer thickness of the crust.

### 5.1. Regional Patterns in Fault Orientation

Using relocated earthquakes and the extended focal mechanism catalog, we interpret and categorize the motion on previously known faults (i.e., Totschunda and Duke River faults) as well as newly mapped faults (Figure 4a). The predominance of strike-slip and reverse faulting focal mechanisms indicates a transpressional regime in southwest Yukon, consistent with previous characterizations of the region near the indentor corner (Choi et al., 2021; Marechal et al., 2015) and more directly along the eastern Denali fault (McDermott et al., 2019).

We determine fault plane geometry from focal mechanisms and by analyzing the predominant orientation of seismicity near each focal mechanism. We interpret three regional patterns in fault strike. The predominant faulting direction (Figure 4b), governed by large regional faults, is NW-SE (strike of approximately  $130\text{--}180^{\circ}$  or  $315\text{--}350^{\circ}$ ). This is most apparent for dextral strike-slip faulting (Figure 4c), but a subset of reverse faults also approximately exhibit this strike orientation. Interpreted faults identified in this category would include the Totschunda fault and the Connector fault. Second, we observe E-W strike orientations (strike of approximately  $90\text{--}135^{\circ}$  or  $260\text{--}300^{\circ}$ ) seen in Figures 4b and 4d. The E-W faulting is predominantly observed in reverse faulting mechanisms (with some strike-slip events). These faults include the active portion of the Duke River and

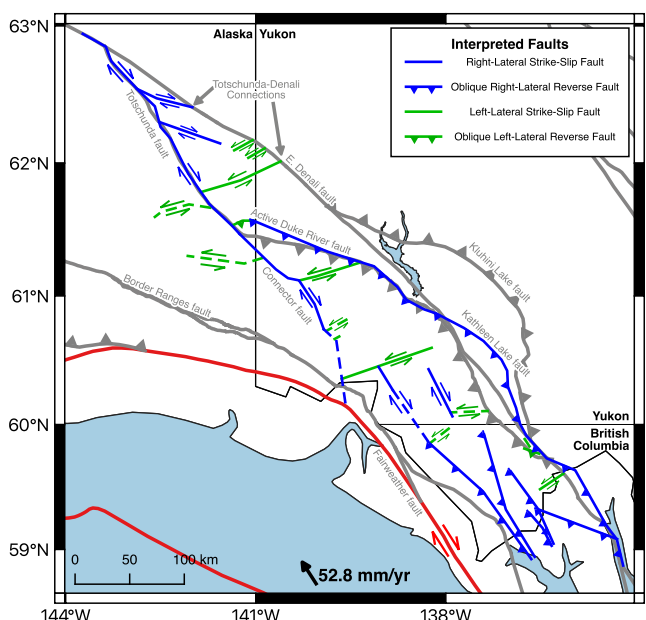


**Figure 6.** Interpreted faults with fault motions showing the distribution of dextral (blue) and sinistral (green) fault motions on strike-slip and reverse faults. Dashed lines indicate uncertain fault locations due to limited seismicity. Known regional faults can be seen in gray, and plate boundary faults and fault motion are in red. Yakutat motion indicated by arrow (Elliott & Freymueller, 2020).

lateral faults occur at a high angle to the bounding Totschunda and Denali faults and occur across the entire study region between the Connector fault and the Duke River fault, and even west of the Connector fault (Figure 6). The NW striking right lateral faults are observed within the entire area, forming a nested network of faults, including in the proposed location of the Connector fault (Figure 6). However, there is no evidence of discrete through-going deformation occurring over the entire connected portion of the Connector fault. Another set of NW striking right lateral faults lies inboard of the northern Fairweather fault (Figure 6). These faults transition to oblique reverse faults further south in the study area. There is a general lack of strike-slip motion along the Denali fault in the southeast corner of our study area, consistent with previous studies (Choi et al., 2021).

We observe significant seismicity near the Duke River fault (Figure 6). However, the majority of events lie along a quasi-linear feature north of the surface trace of the northern Duke River fault. This discrete fault diverges from the Totschunda at approximately 61.5°N as a left-lateral oblique reverse fault striking to the NE (green line in Figure 6). Seismicity then extends to the southeast as an NW striking right-lateral oblique reverse fault and connects with the surface trace of the Duke River fault at approximately 139°W. Thrust faulting continues along the Duke River fault for 100 km. South of Kluane Lake, active faulting continues in a NW-SE strike across and east of the Denali fault before curving southward along the deformation front as a right-lateral oblique reverse fault. This structure, which we name the Kathleen Lake fault (Figure 6), is consistent with a change in topographic relief along the deformation front (Figure 4a). Interestingly, we observe minimal seismicity along the southern portion of the Duke River fault or the Eastern Denali fault. The Kathleen Lake fault deviates from the Denali fault at 60.8°N and reconnects with the Denali fault further south at about 60°N, near the location of the St. Elias earthquake doublet. The Kathleen Lake fault exhibits a similar arch shape as larger faults, including the Kluhini River fault (a major Cenozoic thrust fault; Figure 1) and the Shakwak fault (Israel et al., 2014), as well as the general Cordilleran deformation front in the Mackenzie Mountains (Estève et al., 2021) supporting a contractional component.

The existence of a Totschunda-Fairweather connection (Connector fault) has been speculated for decades (Richter & Matson, 1971). This study presents clear evidence for its existence in terms of focal mechanisms and earthquake locations (Figure 4a). Based on our results, we interpret the Connector fault as an active, dextral strike-slip fault system (Figure 6). Its location is from the southern end of the Totschunda fault, where it meets the Duke

Kathleen Lake faults. The third observed pattern is sinistral strike-slip motion occurring on faults oriented WSW-ENE with strikes ranging from 50 to 90° and 230–270° (Figure 4c). These faults represent interpreted structures connecting the Totschunda and Eastern Denali faults, and the Connector and Duke River faults.

From analysis of strike-slip focal mechanisms (Figure 4c), we observe two subsets of strike-slip events: (a) dextral events on NW striking regional bounding faults and (b) sinistral events on subsidiary ENE striking faults. Sinistral strike-slip faults connected to the major regional faults include faults between the Totschunda and Denali faults and sub-faults from the Connector fault. The orientation of these faults suggests that the areas between the Totschunda-Fairweather system and the Denali fault currently deform as independent blocks. We interpret that the few normal faulting mechanisms (Figure 4d) observed are consistent with the transpressional nature of the study region. These are generally observed near the corners of fault-bounded blocks (see Figure S2D in Supporting Information S1). Yet, we observe no regionally consistent pattern in their orientations. However, one location where we see several consistent normal focal mechanisms is the southern end of the Connector fault, south of 61°N. Based on block models, extension is expected on the Connector fault at a rate of 2 mm/yr (Elliott & Freymueller, 2020), and therefore, these results are consistent with previous models of the fault's motion.

In the northern part of the study area, we identified two NW-SE striking right lateral and WSW-ENE striking left lateral faults between the Totschunda and Eastern Denali faults, suggesting a kinematic link between the two fault systems (Figure 6). These faults are predominantly strike-slip faults. Left

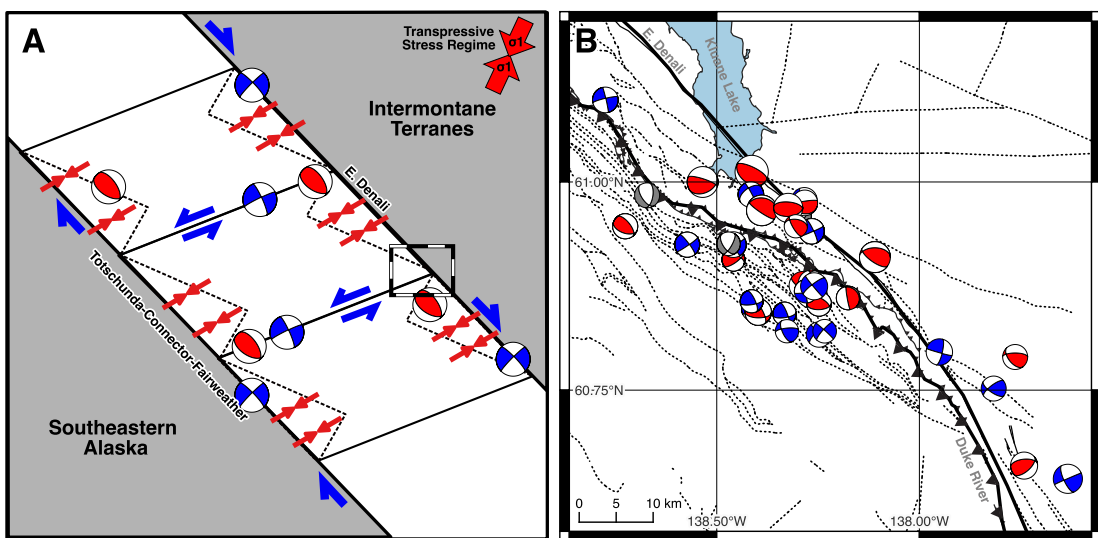


**Figure 7.** (a) Interpretive simplified schematic of regional faulting in a transpressional setting with localized stress orientation estimates from the World Stress Map (Heidbach et al., 2018). Strike-slip and reverse motion are shown in blue and red, respectively, with associated focal mechanisms. Transpression causes shortening of internal rock masses (dashed lines; Zuza & Yin, 2016) as well as slip partitioning near boundaries. (b) Deformation at fault intersections (inset location shown in panel a) can exhibit partitioning of slip as both reverse (red) and strike-slip (blue) events over a local-scaled, densely faulted (dashed lines; Colpron, 2022) junction between the Duke River Fault and Eastern Denali Fault (black lines). Normal focal mechanisms shown in gray.

River fault, to the crossing of the Border Ranges fault, and finally connecting to the Fairweather fault (Figure 6). While there are limited available focal mechanisms for the southern portion of this fault (south of 61°N), sufficient focal mechanisms exist in the northern portion of the fault to characterize the motion as right-lateral. There are multiple ENE striking left-lateral strike-slip faults attached to the Connector fault, suggesting additional connections to the Duke River fault system.

## 5.2. Evidence for Active Discrete and Distributed Deformation on a Regional Scale

The geologic structures in southwest Yukon are dominated by a complex fold and thrust belt and large displacement dextral strike-slip faulting systems. We observe that active deformation occurs within a complex network of distributed deformation and along discrete structures throughout the region bounded by the eastern Denali (to the east) and the Fairweather-Connector-Totschunda fault system (to the west). While these serve as major regional fault systems separately, they are also connected by a series of minor faults that form a complex fault network within a corridor of active deformation (Figure 6).

We present an interpretation of this corridor of deformation as part of the larger Yakutat-North American collision (Figure 7a), with localized areas of slip partitioning based on the seismic evidence. For example, the seismicity to the SW of the Totschunda-Connector bounding fault highlights that active deformation occurs beyond our study area, with most of the compression accommodated southwest of the plate boundary. The overall direction of slip follows the regional dextral NW-SE faulting. The interior of this corridor is transected by sinistral faults oriented NE-SW, delineating blocks that rotate clockwise. Since southeast Alaska and southwest Yukon are in a transpressional stress regime, the intervening crust exhibits shortening, both internal and along their margins (Zuza & Yin, 2016), leading to a combination of reverse and strike-slip events in these regions (Dickinson, 1996; Page et al., 1995). Although the actual deformation processes are significantly more complex than what is illustrated in Figure 7a, we present a possible simplified schematic to draw comparisons and highlight first-order observations in our interpreted regional fault network (Figure 6). One notable complexity of this system is the presence of thrust and reverse faults, like the Duke River fault, which are internal to the larger regional model but cut across multiple blocks in this zone.

At a local scale (Figure 7b), these faults exhibit distributed deformation occurring over a zone tens of kilometers wide. In locations that are well mapped, like the southern end of Kluane Lake, this coincides with a highly faulted region. Notably, our focal mechanism catalog shows evidence for slip-partitioning, either as pure reverse mechanisms or pure strike-slip mechanisms, near fault intersections. Slip-partitioning is consistent with other

regional studies, which show outcrop evidence for geologically young slip-partitioning on the Denali fault (McDermott et al., 2021) as well as slip-partitioning in notable recent earthquakes such as the 2002 Denali event (Eberhart-Phillips et al., 2003) and the 2017 St. Elias events (Choi et al., 2021; He et al., 2018).

Our data indicate that seismicity over the last decade is clustered along a network of well-defined upper-crustal faults outlining a series of fault-bounded deforming blocks throughout the region. Strain is being distributed inboard of the Yakutat-North American margin from the Fairweather-Connector-Totschunda system to the Denali fault and beyond (e.g., Kathleen Lake fault). These results represent a snapshot of current, active deformation that show clear evidence of reactivation of older structures such as portions of the Duke River fault and the formation of new strike-slip and reverse faults that have not been recognized.

We find clear seismic evidence for the presence, location, and orientation of the dextral Connector fault system that links the Totschunda and Fairweather faults and varies in strike from NNW to NW (Figure 6). The eastern boundary of this deformation zone only locally coincides with the surface expression of the eastern Denali fault, but new faults, such as the Kathleen Lake fault, show that the boundary may coincide with the topographic boundary of the Kluane Ranges, reflecting the overall contraction of the region. The observed deformation may be a reflection of an evolving deformation pattern that is the result of the increased coupling between the colliding Yakutat and North American plate. Offshore seismic studies across the Yakutat microplate revealed that the thickness of the Yakutat basement increases and the overlying sedimentary cover decreases from 15 km thickness in the NW to less than 5 km in the SE, which indicates significant changes to the incoming rheology (Van Avendonk et al., 2013). This assertion is supported by thermochronological evidence that revealed the change in the rock uplift and erosion through late Cenozoic time (roughly 4 to 2 Ma; Enkelmann et al., 2015). The fact that thermochronometric cooling ages suggest that there was no more than 2–3 km of erosion inboard of the Connector fault (Enkelmann et al., 2017) suggests that our observed transpressional deformation in SW Yukon must be young.

### 5.3. Constraining the Crustal Seismogenic Layer Thickness

Seismicity largely occurs in the brittle regime of the Earth's crust and, therefore, estimates of seismogenic thickness can be used to define the brittle-plastic transition (Furlong & Atkinson, 1993; Hyndman, 2023; Miller & Furlong, 1988). This allows us to place constraints on the thermal structure of the crust inboard of the Yakutat indentor corner as the brittle-plastic transition is a thermal rheological transition which occurs at approximately 350°C for quartz-felspathic continental crusts (Hyndman et al., 1997; Sibson, 1982).

Our relocated catalog significantly improves earthquake depth estimates and improves the estimation of the depth extent of the crustal seismogenic thickness. Figure 8 shows a comparison of our estimates of seismogenic layer thickness to inferred Curie-depth throughout southeast Alaska and southwest Yukon. Seismogenic layer thicknesses were taken as the depth comprising 90% of seismicity (Furlong & Atkinson, 1993; Miller & Furlong, 1988; Smith-Konter et al., 2011) in overlapping spatial bins of 35 km in lateral extent. Curie-depths provide a constraint on the maximum depth of magnetization in the crust, which occurs at a temperature of approximately 570°C for magnetite (the dominant magnetic mineral). For comparison, Curie-depths were extracted from a global model (Li et al., 2017) and averaged over the same spatial bins. The shallowest estimates of seismogenic thickness (8.5 km) are observed in the complex region where the eastern Denali, Duke River, and Kathleen Lake faults are all in proximity to one another with other unnamed faults in the southern end of the study region (approx. 60°N and 137°W). The deepest estimates (19 km) are observed along the northern Fairweather fault and suggests that the edge of the subducting Yakutat slab (as outlined in Figure 1a) may cool the crust, resulting in a thicker seismogenic layer.

The thin seismogenic layer thicknesses (9–13 km) observed throughout the study region (Table 2 and Figure 8a) suggest high crustal temperatures. This is consistent with other geophysical observations, including global models of Curie-depths, which are estimated to be around 10–16 km throughout the study region (Figure 1b and Figure 8b; Li et al., 2017). However, Curie depth estimates have gaps near the Connector fault (Figure 1b; Li et al., 2017) due to limitations in remote-sensing methods. Overall, our results are also consistent with large-scale estimates of the effective elastic thickness of the lithosphere of <20 km (Hyndman et al., 2005), elevated Moho temperature estimates of 800–1,000°C (Hyndman et al., 2005), and evidence of a shallow lithosphere–asthenosphere boundary for the entire Northern Canadian Cordillera (O'Driscoll & Miller, 2015). Ultimately, earthquake relocations support previous understanding of elevated geothermal gradients in the northern Canadian

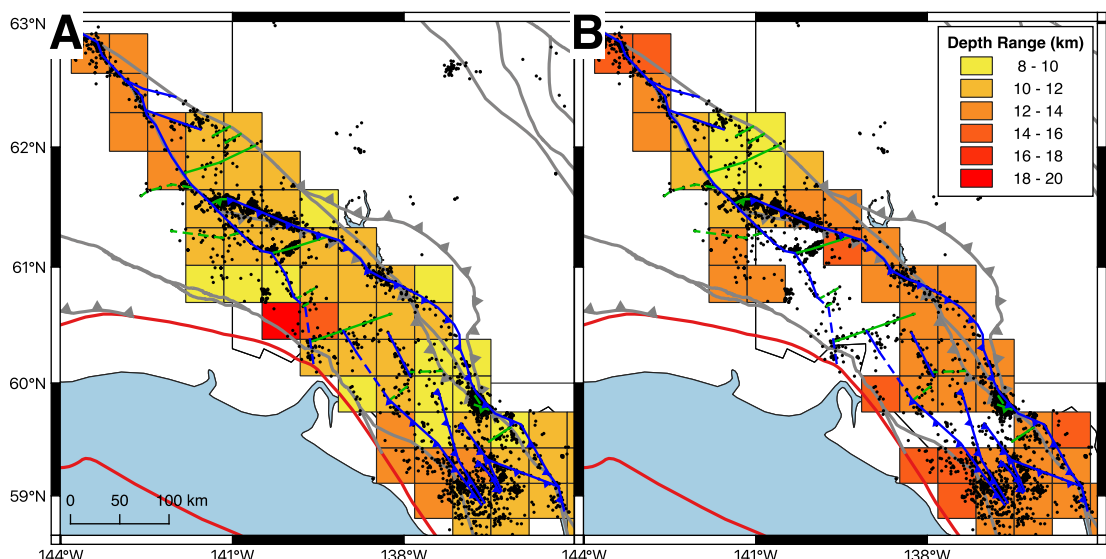


**Figure 8.** (a) Seismogenic layer thickness estimates from relocated earthquakes compared to (b) Curie-depth estimates averaged over the same spatial grid (Li et al., 2017). The color-depth scale is the same for both maps. Relocated seismicity (black dots), major regional faults, and interpreted faults are also shown (colored as in Figure 6).

Cordillera compared to typical continental crust (Hyndman et al., 2005), as well as models that suggest elevated basal temperatures enable inland stress transfer (Mazzotti & Hyndman, 2002).

## 6. Conclusions

This study presents a catalog of relocated seismicity containing 5,536 events for southeast Alaska and southwest Yukon between 2010 and 2021. This relocated catalog provides better relative event locations, reducing event-pair residuals and creating clearer images of seismicity. We also improve absolute event locations in the catalog, as evidenced by a reduction in RMS misfit. These catalog improvements allow us to better evaluate earthquake locations, particularly their depths, which we use to estimate the seismogenic thickness of the crust. Seismicity in southwest Yukon is shallow, with seismogenic thicknesses ranging from 9 to 19 km, depending on the location. These results also support previous studies indicating an elevated geothermal gradient throughout the region.

By studying a combination of earthquake relocations and focal mechanisms, we identify active fault orientations and classify their motions. Fault strike orientations are primarily NW-SE, aligned with the major regional fault structures such as the eastern Denali and Fairweather faults. We find a subset of reverse faults oriented E-W and a set of sinistral strike-slip faults oriented NE-SW linking the major structures in a complex manner. This includes links between the Totschunda and eastern Denali faults (north of 61.65°N), the Duke River fault and other similarly oriented thrust faults, and faults connecting the Fairweather and eastern Denali systems (south of 61.5° N). This complex fault network includes the speculated Connector fault, for which we show clear evidence of its

existence, connecting the Totschunda and Fairweather faults. These results highlight that active deformation is more complex than what can be described by known or mapped faults and indicates the presence of new structures, deviations from known structures, and reactivation of old structures.

Seismicity in southwest Yukon reflects a corridor of deformation characterized by a network of upper crustal faults. At a large scale, active deformation is predominantly bounded by the Totschunda-Connector-Fairweather fault system (to the west) and the eastern Denali and Kathleen Lake faults (to the east), with rotating blocks in between that are delineated by NW-SE striking sinistral faults. However, we note seismicity immediately to the southwest of these bounding fault systems which highlights how deformation within our study area acts within a larger tectonic context. The transpressional stress

**Table 2**  
*Estimates of Crustal Seismogenic Layer Thickness Near Various Fault Segments*

Fault segment	Seismogenic layer thickness of crust (km)
Totschunda	12.8
Totschunda - Denali Corridor	10.3
Duke River (West)	11.4
Connector	9.0
Duke River (East)	10.7

regime from the colliding Yakutat microplate causes oblique reverse mechanisms and localized slip partitioning that lead to high topography. Overall, our results indicate deformation along discrete major structures, as well as more distributed deformation in a complex network of intra-corridor transecting faults that is consistent with a complex history of deformation in the region that likely continues to evolve in the present day.

## Data Availability Statement

Seismic data used in this study were accessed through the EarthScope Consortium Web Services (<https://service.iris.edu/>), including the following seismic networks: AK (Alaska Regional; Alaska Earthquake Center, 1987), AT (Alaska Tsunami; National Oceanic and Atmospheric Administration (NOAA), 1967), CN (Canadian National; National Resources Canada (NRCan), 1975), NY (Yukon-Northwest; University of Ottawa, 2013), and TA (Transportable Array; IRIS Transportable Array, 2003). The starting earthquake locations are part of the comprehensive earthquake catalog (ComCat) and were downloaded via Earthscope Web Services (U.S. Geological Survey, 2022). Relocated earthquake events and the focal mechanism catalog discussed in this manuscript are included in the Supporting Information (Data Sets S1 and S2). Focal mechanisms were taken from a variety of sources, including the ComCat (via EarthScope Web Services; U.S. Geological Survey, 2022), International Seismological Centre (ISC; Lendas et al., 2019), and St. Louis University (Herrmann et al., 2011). The small magnitude focal mechanism catalog used in this work was first published in Gosselin et al. (2023). The software used in this analysis is open source. For relocating events, we used a Python implementation of double-difference relocation (<https://github.com/katie-biegel/relocDD-py>; Biegel & Dettmer, 2024). Focal mechanisms were processed using FMC (<https://github.com/Jose-Alvarez/FMC>; Alvarez-Gomez, 2019). The basemap layer used in several of the figures is the ESRI Oceans basemap (ESRI, 2016). Maps were produced using QGIS software (v3.30.2; QGIS.org, 2024).

## Acknowledgments

The authors would like to thank the reviewers at both the journal and the USGS for their comments that helped improve this manuscript. This research was supported by the Yukon Geological Survey, an Alliance Grant ALLRP-80887-22 from the Natural Sciences and Engineering Research Council of Canada (NSERC), and by an NSERC Discovery Grant to Jan Dettmer. Additional scholarship funding for Katherine Biegel was provided by Alberta Innovates and the Society of Exploration Geophysicists. J.S. Caine contributions are supported by the U.S. Geological Survey, Mineral Resources Program. Any use of trade, firm, or product names is for descriptive purposes only and does not imply endorsement by the U.S. Government. This is Yukon Geological Survey contribution #067.

## References

- Alaska Earthquake Center. (1987). Alaska geophysical network (AK) [Dataset]. *University of Alaska Fairbanks: International Federation of Digital Seismograph Networks*. <https://doi.org/10.7914/SN/AK>
- Alvarez-Gomez, J. A. (2019). FMC—Earthquake focal mechanisms data management, cluster and classification. *SoftwareX*, 9, 299–307. <https://doi.org/10.1016/j.softx.2019.03.008>
- Aster, R., Borchers, B., & Thurber, C. (2018). *Parameter estimation and inverse problems*. Academic Press.
- Audet, P., Schutt, D. L., Schaeffer, A. J., Estéve, C., Aster, R. C., & Cubley, J. F. (2020). Moho Variations across the northern Canadian cordillera. *Seismological Research Letters*, 91(6), 3076–3085. <https://doi.org/10.1785/0220200166>
- Biegel, K., & Dettmer, J. (2024). relocDD-py [Software]. Zenodo. <https://doi.org/10.5281/zenodo.10607406>
- Bruhn, R. L., Sauber, J., Cotton, M. M., Pavlis, T. L., Burgess, E., Ruppert, N., & Forster, R. R. (2012). Plate margin deformation and active tectonics along the northern edge of the Yakutat terrane in the Saint Elias Orogen, Alaska, and Yukon, Canada. *Geosphere*, 8(6), 1384–1407. <https://doi.org/10.1130/GES00807.1>
- Brunn, T. R. (1983). Model for the origin of the Yakutat block, an accreting terrane in the northern Gulf of Alaska. *Geology*, 11(12), 718–721. [https://doi.org/10.1130/0091-7613\(1983\)11\(718:MFTOOT\)2.0.CO;2](https://doi.org/10.1130/0091-7613(1983)11(718:MFTOOT)2.0.CO;2)
- Choi, M., Eaton, D. W., & Enkelmann, E. (2021). Is the Eastern Denali fault still active? *Geology*, 49(6), 662–666. <https://doi.org/10.1130/G48461.1>
- Christeson, G. L., Gulick, S. P., van Avendonk, H. J., Worthington, L. L., Reece, R. S., & Pavlis, T. L. (2010). The Yakutat terrane: Dramatic change in crustal thickness across the Transition fault, Alaska. *Geology*, 38(10), 895–898. <https://doi.org/10.1130/G31170.1>
- Cobbett, R., Israel, S., Mortenson, J., Joyce, N., & Crowley, J. (2016). Structure and kinematic evolution of the Duke River fault, southwestern Yukon. *Canadian Journal of Earth Sciences*, 54(3), 322–344. <https://doi.org/10.1139/cjes-2016-0074>
- Colpron, M. (2022). The Yukon digital bedrock geology compilation. In K. MacFarlane (Ed.), *Yukon Exploration and Geology 2021* (pp. 143–159). Yukon Geological Survey.
- Colpron, M., & Nelson, J. (2020). *A digital atlas of terranes for the northern Cordillera*. (Tech. Rep.). Yukon Geological Survey. Retrieved from <http://data.geology.gov.yk.ca/Compilation/2>
- Davis, T. N., & Sanders, N. K. (1960). Alaska earthquake of July 10, 1958: Intensity distribution and field investigation of Northern Epicentral region. *Bulletin of the Seismological Society of America*, 50(2), 221–252. <https://doi.org/10.1785/BSSA0500020221>
- Dickinson, W. R. (1996). *Kinematics of transrotational tectonism in the California transverse ranges and its contribution to cumulative slip along the San Andreas transform fault system* (Vol. 305). Geological Society of America. <https://doi.org/10.1130/0-8137-2305-1.1>
- Dodds, C., & Campbell, R. (1992). Overview, legend, and mineral deposit tabulations for geolog of SW Kluane Lake, Mount Saint Elias, SW Dezadeash, NW Yakutat, and Tatshenini map areas. Yukon Territory and British Columbia (Open File Report No. 2188-2191). Geological Survey of Canada.
- Doser, D. (2010). A re-evaluation of the 1958 Fairweather, Alaska, earthquake. *Bulletin of the Seismological Society of America*, 100(4), 1792–1799. <https://doi.org/10.1785/0120090343>
- Doser, D. (2012). Revisiting the 1979 St. Elias, Alaska, aftershock sequence and its regional significance. *Bulletin of the Seismological Society of America*, 102(6), 2392–2404. <https://doi.org/10.1785/0120120007>
- Doser, D. (2014). Seismicity of Southwestern Yukon, Canada, and its relation to slip transfer between the Fairweather and Denali fault systems. *Tectonophysics*, 611, 121–129. <https://doi.org/10.1016/j.tecto.2013.11.018>
- Doser, D., & Lomas, R. (2000). The transition from strike-slip to oblique subduction in Southeastern Alaska from seismological studies. *Tectonophysics*, 316(1–2), 45–65. [https://doi.org/10.1016/S0040-1951\(99\)00254-1](https://doi.org/10.1016/S0040-1951(99)00254-1)

- Doser, D., Pelton, J. R., & Veilleux, A. M. (1997). Earthquakes in the Pamplona zone, Yakutat block, south central Alaska. *Journal of Geophysical Research*, 102(B11), 24499–24511. <https://doi.org/10.1029/97JB01729>
- Eberhart-Phillips, D., Christensen, D. H., Brocher, T. M., Hansen, R., Ruppert, N. A., Haeussler, P. J., & Abers, G. A. (2006). Imaging the transition from Aleutian subduction to Yakutat collision in central Alaska, with local earthquakes and active source data. *Journal of Geophysical Research*, 111(B11). <https://doi.org/10.1029/2005JB004240>
- Eberhart-Phillips, D., Haeussler, P. J., Freymueller, J. T., Frankel, A. D., Rubin, C. M., Craw, P., et al. (2003). The 2002 Denali Fault earthquake, Alaska: A large magnitude, slip-partitioned event. *Science*, 300(5622), 1113–1118. <https://doi.org/10.1126/science.1082703>
- Elliott, J., & Freymueller, J. T. (2020). A block model of present-day kinematics of Alaska and western Canada. *Journal of Geophysical Research: Solid Earth*, 125(7), e2019JB018378. <https://doi.org/10.1029/2019JB018378>
- Enkelmann, E., Koons, P., Pavlis, T. L., Hallet, B., Barker, A., Elliott, J., et al. (2015). Cooperation among tectonic and surface processes in the St. Elias Range, Earth's highest coastal mountains. *Geophysical Research Letters*, 42(14), 5838–5846. <https://doi.org/10.1002/2015GL064727>
- Enkelmann, E., Piestrzeniewicz, A., Falkowski, S., Stübner, K., & Ehlers, T. A. (2017). Thermochronology in southeast Alaska and southwest Yukon: Implications for North American Plate response to terrane accretion. *Earth and Planetary Science Letters*, 457, 348–358. <https://doi.org/10.1016/j.epsl.2016.10.032>
- Enkelmann, E., Zeitler, P., Pavlis, T., Gerver, J., & Ridgway, K. (2009). Intense localized rock uplift and erosion in the St Elias Orogen of Alaska. *Nature Geoscience*, 2(5), 360–363. <https://doi.org/10.1038/ngeo502>
- ESRI. (2016). Ocean basemap [Dataset]. United States of America: ESRI. [https://services.arcgisonline.com/ArcGIS/rest/services/Ocean/World\\_Ocean\\_Base/MapServer/tile/%7Bz%7D/%7By%7D/%7Bx%7D](https://services.arcgisonline.com/ArcGIS/rest/services/Ocean/World_Ocean_Base/MapServer/tile/%7Bz%7D/%7By%7D/%7Bx%7D)
- Estève, C., Gosselin, J. M., Audet, P., Schaeffer, A. J., Schutt, D. L., & Aster, R. C. (2021). Surface-wave tomography of the northern Canadian cordillera using earthquake Rayleigh wave group velocities. *Journal of Geophysical Research: Solid Earth*, 126(8), e2021JB021960. <https://doi.org/10.1029/2021JB021960>
- Fogleman, K. A., Lahr, J. C., Stephens, C. D., & Page, R. A. (1993). *Earthquake locations determined by the southern Alaska seismograph network for October 1971 through May 1989* (Tech. Rep. No. 93-309). USGS. <https://doi.org/10.3133/ofr93309>
- Furlong, K. P., & Atkinson, S. M. (1993). Seismicity and thermal structure along the northern San Andreas fault system, California, USA. *Tectonophysics*, 217(1–2), 23–30. [https://doi.org/10.1016/0040-1951\(93\)90199-T](https://doi.org/10.1016/0040-1951(93)90199-T)
- Gosselin, J. M., Biegel, K. M., Hamidbeygi, M., & Dettmer, J. (2023). Improvements in the regional earthquake focal mechanism catalogue for southwestern Yukon. In K. MacFarlane (Ed.), *Yukon Exploration and Geology 2022* (pp. 63–76). Yukon Geological Survey.
- Haeussler, P. J., Schwartz, D. P., Dawson, T. E., Stenner, H. D., Lienkaemper, J. J., Cinti, F., et al. (2004). Surface rupture of the 2002 Denali fault, Alaska, earthquake and comparison to other strike-slip ruptures. *Earthquake Spectra*, 20(3), 565–578. <https://doi.org/10.1193/1.1775797>
- Hardebeck, J. L., & Shearer, P. M. (2002). A new method for determining first-motion focal mechanisms. *Bulletin of the Seismological Society of America*, 92(6), 2264–2276. <https://doi.org/10.1785/0120010200>
- He, X., Ni, S., Zhang, P., & Freymueller, J. (2018). The 1 May 2017 British Columbia-Alaska earthquake doublet and implication for complexity near southern end of Denali fault system. *Geophysical Research Letters*, 45(12), 5937–5947. <https://doi.org/10.1029/2018GL078014>
- Heidbach, O., Rajabi, M., Cui, X., Fuchs, K., Müller, B., Reinecker, J., et al. (2018). The World Stress Map database release 2016: Crustal stress pattern across scales. *Tectonophysics*, 744, 484–498. <https://doi.org/10.1016/j.tecto.2018.07.007>
- Herrmann, R., Benz, H., & Ammon, C. (2011). Monitoring the earthquake process in North America. *Bulletin of the Seismological Society of America*, 101(6), 2609–2625. <https://doi.org/10.1785/0120110095>
- Hyndman, R. (2023). The thermal regime of NW Canada and Alaska, and tectonic and seismicity consequences. *Geochemistry, Geophysics, Geosystems*, 24(7). <https://doi.org/10.1029/2022GC010570>
- Hyndman, R., Flück, P., Mazzotti, S., Lewis, T. J., Ristau, J., & Leonard, L. (2005). Current tectonics of the northern Canadian Cordillera. *Canadian Journal of Earth Sciences*, 42(6), 1117–1136. <https://doi.org/10.1139/e05-023>
- Hyndman, R., Yamano, M., & Oleskevich, D. A. (1997). The seismogenic zone of subduction thrust faults. *Island Arc*, 6(3), 244–260. <https://doi.org/10.1111/j.1440-1738.1997.tb00175.x>
- IRIS Transportable Array. (2003). USArray transportable Array (EarthScope TA) [Dataset]. International Federation of Digital Seismograph Networks. <https://doi.org/10.7914/SN/TA>
- Israel, S., Colpron, M., Cubley, J., Moynihan, D., Murphy, D., & Relf, C. (2014). *Preliminary bedrock geology of the Mt. Decoeli area (Parts of NTS 115A/12, 13 and 115B/9, 16)* (Tech. Rep. No. 2014-18). Yukon Geological Survey. Retrieved from <http://data.geology.gov.yk.ca/Compilation/2>
- Kalbas, J. L., Freed, A. M., & Ridgway, K. D. (2008). Contemporary fault mechanics in southern Alaska. In J. T. Freymueller, P. J. Haeussler, R. L. Wesson, & G. Ekström (Eds.), *Geophysical monograph series* (pp. 321–336). American Geophysical Union. <https://doi.org/10.1029/179GM18>
- Koons, P., Hallet, B., Zeitler, P. K., & Meltzer, A. S. (2022). Tectonic aneurysm: A culmination of tectonic and geomorphic cooperation in mountain building. In J. J. F. Shroder (Ed.), *Treatise on geomorphology* (2nd ed., pp. 695–728). Academic Press. <https://doi.org/10.1016/B978-0-12-818234-5.00179-6>
- Koons, P., Hooks, B., Pavlis, T., Upton, P., & Barker, A. (2010). Three-dimensional mechanics of Yakutat convergence in the southern Alaskan plate corner. *Tectonics*, 29(4). <https://doi.org/10.1029/2009TC002463>
- Lentas, K., Di Giacomo, D., Harris, J., & Storchak, D. (2019). The ISC Bulletin as a comprehensive source of earthquake source mechanisms. *Earth System Science Data*, 11(2), 565–578. <https://doi.org/10.5194/essd-11-565-2019>
- Li, C.-F., Lu, Y., & Wang, J. (2017). A global reference model of Curie-point depths based on EMAG2. *Scientific Reports*, 7(1), 45129. <https://doi.org/10.1038/srep45129>
- Lowey, G. W. (1998). A new estimate of the amount of displacement on the Denali fault system based on the occurrence of carbonate mega-boulders in the Dezadeash formation (Jura-Cretaceous), Yukon, and the Nutzotin mountains sequence (Jura-Cretaceous), Alaska. *Bulletin of Canadian Petroleum Geology*, 46(3), 379–386. <https://doi.org/10.35767/gscpbull.46.3.379>
- Ma, S., & Audet, P. (2017). Seismic velocity model of the crust in the northern Canadian Cordillera from Rayleigh wave dispersion data. *Canadian Journal of Earth Sciences*, 54(2), 163–172. <https://doi.org/10.1139/cjes-2016-0115>
- Marechal, A., Mazzotti, S., Elliott, J. L., Freymueller, J. T., & Schmidt, M. (2015). Indentor-corner tectonics in the Yakutat-St. Elias collision constrained by GPS. *Journal of Geophysical Research: Solid Earth*, 120(5), 3897–3908. <https://doi.org/10.1002/2014JB011842>
- Marechal, A., Ritz, J.-F., Ferry, M., Mazzotti, S., Blard, P.-H., Braucher, R., & Saint-Carlier, D. (2018). Active tectonics around the Yakutat indentor: New geomorphological constraints on the eastern Denali, Totschunda and Duke River Faults. *Earth and Planetary Science Letters*, 482, 71–80. <https://doi.org/10.1016/j.epsl.2017.10.051>
- Mazzotti, S., & Hyndman, R. (2002). Yakutat collision and strain transfer across the northern Canadian Cordillera. *Geology*, 30(6), 495–498. [https://doi.org/10.1130/0091-7613\(2002\)030\(0495:YCASTA\)2.0.CO;2](https://doi.org/10.1130/0091-7613(2002)030(0495:YCASTA)2.0.CO;2)

- McDermott, R. G., Ault, A. K., & Caine, J. S. (2021). Dating fault damage along the eastern Denali fault zone with hematite (U-Th)/He thermochronometry. *Earth and Planetary Science Letters*, 563, 116872. <https://doi.org/10.1016/j.epsl.2021.116872>
- McDermott, R. G., Ault, A. K., Caine, J. S., & Thomson, S. N. (2019). Thermotectonic history of the Kluna ranges and evolution of the eastern Denali fault zone in southwestern Yukon, Canada. *Tectonics*, 38(8), 2983–3010. <https://doi.org/10.1029/2019TC005545>
- Meighan, L. N., Cassidy, J. F., Mazzotti, S., & Pavlis, G. L. (2013). Microseismicity and tectonics of Southwest Yukon territory, Canada, using a local dense seismic array. *Bulletin of the Seismological Society of America*, 103(6), 3341–3346. <https://doi.org/10.1785/0120130068>
- Menke, W., & Schaff, D. (2004). Absolute earthquake locations with differential data. *Bulletin of the Seismological Society of America*, 94(6), 2254–2264. <https://doi.org/10.1785/0120040033>
- Miller, C. K., & Furlong, K. P. (1988). Thermal-mechanical controls on seismicity depth distributions in the San Andreas fault zone. *Geophysical Research Letters*, 15(12), 1429–1432. <https://doi.org/10.1029/96GL02066>
- National Oceanic and Atmospheric Administration (NOAA). (1967). National tsunami warning center Alaska seismic network (AT) [Dataset]. *International Federation of Digital Seismograph Networks*. <https://doi.org/10.7914/SN/AT>
- National Resources Canada (NRCCAN). (1975). Canadian National Seismograph network (CNSN) [Dataset]. *International Federation of Digital Seismograph Networks*. <https://doi.org/10.7914/SN/CN>
- O'Driscoll, L. O., & Miller, M. S. (2015). Lithospheric discontinuity structure in Alaska, thickness variations determined by  $s_p$  receiver functions. *Tectonics*, 34(4), 694–714. <https://doi.org/10.1002/2014TC003669>
- Page, R. A., Plafker, G., & Pulpan, H. (1995). Block rotation in east-central Alaska: A framework for evaluating earthquake potential? *Geology*, 23(7), 629–632. [https://doi.org/10.1130/0091-7613\(1995\)023\(0629:BRIECA\)2.3.CO;2](https://doi.org/10.1130/0091-7613(1995)023(0629:BRIECA)2.3.CO;2)
- Paige, C. C., & Saunders, M. A. (1982). LSQR: An algorithm for sparse linear equations and sparse least squares. *ACM Transactions on Mathematical Software*, 8(1), 43–71. <https://doi.org/10.1145/355984.355989>
- Plafker, G. (1987). Regional geology and petroleum potential of the northern Gulf of Alaska continental margin. In D. W. Scholl, A. Grantz, & J. G. Vedder (Eds.), *Geology and resource potential of the continental margin of western north America and adjacent ocean basins - Beaufort sea to Baja California* (Vol. 6, pp. 229–268). Circum-Pacific Council for Energy and Mineral Resources Earth Science Series.
- Plafker, G., & Thatcher, W. (2008). Geological and geophysical evaluation of the mechanisms of the great 1899 Yakutat bay earthquakes. *Active Tectonics and Seismic Potential of Alaska*, 179, 215–236. <https://doi.org/10.1029/179GM12>
- QGIS.org. (2024). QGIS geographic information system [Software]. QGIS Association. <https://www.qgis.org>
- Richter, D., & Matson, N. A., JR. (1971). Quaternary faulting in the eastern Alaska range. *GSA Bulletin*, 82(6), 1529–1540. [https://doi.org/10.1130/0016-7606\(1971\)82\[1529:QFITEA\]2.0.CO;2](https://doi.org/10.1130/0016-7606(1971)82[1529:QFITEA]2.0.CO;2)
- Schaeffer, A. J., & Lebedev, S. (2014). Imaging the North American continent using waveform inversion of global and USAArray data. *Earth and Planetary Science Letters*, 402, 26–41. <https://doi.org/10.1016/j.epsl.2014.05.014>
- Shearer, P. M. (1997). Improving local earthquake locations using the L1 norm and waveform cross correlation: Application to the Whittier Narrows, California, aftershock sequence. *Journal of Geophysical Research*, 102(B4), 8269–8283. <https://doi.org/10.1029/96JB03228>
- Sibson, R. (1982). Fault zone models, heat flow, and the depth distribution of earthquakes in the continental crust of the United States. *Bulletin of the Seismological Society of America*, 72(1), 151–163. <https://doi.org/10.1785/BSSA0720010151>
- Smith-Konter, B. R., Sandwell, D. T., & Shearer, P. (2011). Locking depths estimated from geodesy and seismology along the San Andreas Fault System: Implications for seismic moment release. *Journal of Geophysical Research*, 116(B6), B06401. <https://doi.org/10.1029/2010JB008117>
- Stauder, W. (1960). The Alaska earthquake of July 10, 1958: Seismic studies. *Bulletin of the Seismological Society of America*, 50(2), 293–322. <https://doi.org/10.1785/BSSA0500020293>
- Tarr, R., Lawrence, M., & Gilbert, G. K. (1912). The earthquakes at Yakutat bay, Alaska, in September, 1899 (Report No. 69). *United States Geological Survey*. <https://doi.org/10.3133/pp69>
- University of Ottawa. (2013). Yukon-Northwest seismic network (YNSN) [Dataset]. *International Federation of Digital Seismograph Networks*. <https://doi.org/10.7914/SN/NY>
- U.S. Geological Survey. (2022). Advanced national seismic system (ANSS) comprehensive catalog (Comcat) [Dataset]. USGS. <https://doi.org/10.5066/F7MS3QZH>
- Van Avendonk, H. J., Gulick, S. P., Christeson, G. L., Worthington, L. L., Pavlis, T. L., & Ridgway, K. D. (2013). Subduction and accretion of sedimentary rocks in the Yakutat collision zone, St. Elias orogen, Gulf of Alaska. *Earth and Planetary Science Letters*, 381, 116–126. <https://doi.org/10.1016/j.epsl.2013.08.049>
- Vasyura-Bathke, H., Dettmer, J., Steinberg, A., Heimann, S., Isken, M., Zielke, O., et al. (2020). The Bayesian earthquake analysis tool. *Seismological Research Letters*, 91(2A), 1003–1018. <https://doi.org/10.1785/0220190075>
- Waldhauser, F., & Ellsworth, W. L. (2000). A double-difference earthquake location algorithm: Method and application to the northern Hayward fault, California. *Bulletin of the Seismological Society of America*, 90(6), 1353–1368. <https://doi.org/10.1785/0120000006>
- Waldien, T., Roeske, S., & Benowitz, J. (2021). Tectonic underplating and dismemberment of the Maclarens-Kluane schist records late cretaceous terrane accretion polarity and 480 km of post-52 Ma dextral displacement on the Denali fault. *Tectonics*, 40(10). <https://doi.org/10.1029/2020TC006677>
- Walton, M. A., Gulick, S. P., & Haeussler, P. J. (2022). Revisiting the 1899 earthquake series using integrative geophysical analysis in Yakutat Bay, Alaska, USA. *Geosphere*, 18(5), 1453–1473. <https://doi.org/10.1130/GES02423.1>
- Zuza, A. V., & Yin, A. (2016). Continental deformation accommodated by non-rigid passive bookshelf faulting: An example from the cenozoic tectonic development of northern tibet. *Tectonophysics*, 677–678, 227–240. <https://doi.org/10.1016/j.tecto.2016.04.007>